RIS Aided Residual Energy: PS and TS Mode Harvesting in Cooperative Spectrum Sensing

Avik Banerjee,
Department of ECE,
RV College of Engineering,
Bengaluru, Karnataka 560059
Email: avikbanerjee@ieee.org

Prabagarane Nagaradjane,
Department of ECE,
SSN College of Engineering,
Chennai, Tamilnadu-603110
Email: prabagaranen@ssn.edu.in

Santi P Maity,
Department of IT, Indian Institute of
Engineering Science and Technology,
Shibpur, West Bengal 711103
Email: santipmaity@it.iiests.ac.in

Veerapu Goutham,
School of Electronics Engineering,
Vellore Institute of Technology,
Katpadi Tamilnadu-632014
Email: gouthamveerapu@gmail.com

***Abstract*—This work studies performance comparison on radio frequency (RF) energy harvesting (EH) in power splitting (PS) and time switching (TS) modes in reconfigurable intelligent surfaces (RIS) aided cooperative spectrum sensing (CSS). CSS model considers multiple primary user (PU) nodes and a single PU emulation attacker (PUEA) node. A distant dependent model of reflected channel gain in RIS antenna is developed for calculating the harvested residual energy (RE). The primary objective is to maximize the total RE while meeting a predefined detection and false alarm probabilities of PU along with the individual secondary user's (SU's) energy causality constraint. Simulation results show the efficacy of the proposed work due to the involvement of RIS antenna on total RE, as gain of about 45% and 38.97% for PS and TS mode compared to the existing works while maintaining the above mentioned constraints. Performance of RE with the change in the placement of RIS antenna near/far to PU is analyzed for both PS and TS mode.**

***Index Terms*—Cognitive radio, CSS, RIS, EH-CRN, PUEA.**

I. Introduction

Spectrum scarcity, energy crisis, low latency, higher bandwidth, security are the few challenges for upcoming 6G wireless communications [1]. Emergence of Internet of Things (IoT) makes a paradigm shift of human centric mobile communication to connectivity of things and smart devices that are mostly driven by low power battery sources [2]–[4]. The big challenges are power consumption and network connectivity which in turn demand energy and spectrum efficient system design [2], [4]. Spectrum scarcity problems can be addressed using cognitive radio (CR) networks by opportunistically accessing the primary user (PU) spectrum usage [5], [6]. To know about PU spectrum usage activity, cooperative spectrum sensing (CSS), by distributed cognitive users (CRs) is made, where the overall decision of PU transmit or not transmit state over a spectrum band, is decided at fusion center (FC) [6]. Secondary users (SUs) either perform local sensing or may send the amplified version of the PU signal samples to the FC [6]. It is also reported that CSS is prone to several security threats, a commonly used one is primary user emulation attack (PUEA) [6], [7] where a selfish jammer sends a PU-like signal to the FC in order to disrupt the CSS process for own interest [6], [7]. However, PU or PUEA transmission, being broadcast in nature (including jamming signal), radio frequency (RF) signals of the same can be utilized by CR users to perform energy harvesting (EH) [6], [8], [9].

In literature, two types of RF-EH techniques, namely power splitting (PS) [6], [10] and time switching (TS) mode are reported [6], [8]. In PS mode of CR network (CRN) operation, spectrum sensing (SS) and EH are done simultaneously by dividing the received power of PU signal proportionately [6], [10]. In case of TS mode, full portion of the received signal power is used for SS and EH over the non-overlapping time slots [6], [8]. A note worthy results on EH performance comparison results due to PS and TS modes are reported in [6]. To cater passive IoT communications, reconfigurable intelligent surface (RIS) appears as a passive array of relay device to support symbiotic radio (SR) using PU RF wave carrier signal [11]–[13]. RIS possess artificial planar structures, reconfigured and programmable to reflect electromagnetic (EM) waves in a controlled manner [11], [13]. Furthermore, the structure of RIS is handy and light in weight, hence can be deployed in wide variety of environment, like facades of buildings, walls, ceilings, etc [14]. RIS increases coverage of the cells, reduces inter-user interference and improving the security of networks. Although RIS act as passive relay system, it is also explored for performance improvement on EH [11]–[14].

The work in [11] analysed the performance of ergodic capacity considering two separate RISs along with an EH based decode-and-forward (DF) relay. In [12], TS mode based simultaneous wireless information and power transfer (SWIPT) architecture is considered with non-linear (NL) EH at the IoT node. Simulation results in [12] show improved EH performance when the number of elements of RIS is increased. The authors in [13] explored performance of RIS based EH for both linear and NL models where the channels are assumed to follow Nakagami-m fading.

A. Motivation, Scope and Contributions of the Present Work

This paper is an extended version of [6], where a comparative analysis, due to the placement of RIS, on residual energy (RE) for PS and TS based EH operation is done. The major contributions of the paper along with the difference between the present work and [6] are as follows:

- Performance of RE in presence of RIS, multiple PUs and single PUEA is studied here whereas in [6] a single PU and absence of RIS was considered.
- RIS placement on EH performance is studied between the PU transmitter and the receiver (CR node).
- Comparative analysis of PS and TS mode for calculation of RE is analyzed with the change in position of RIS antenna near/far to PU in absence of PUEA.
- Closed form expressions for amplifying gain, total number of SUs, SS duration, and PS ratio (for PS mode) are derived taking RIS sensing channels into consideration and about 45% and 38.97% gain in overall RE for PS and TS mode, respectively are found over [6].

The remainder of the paper is organized as follows: Section II illustrates the system model and frame structure, while RE calculation and problem formulation are done in Section III. Section IV presents numerical results and the paper is concluded in Section V.

II. System Model and Frame Structure

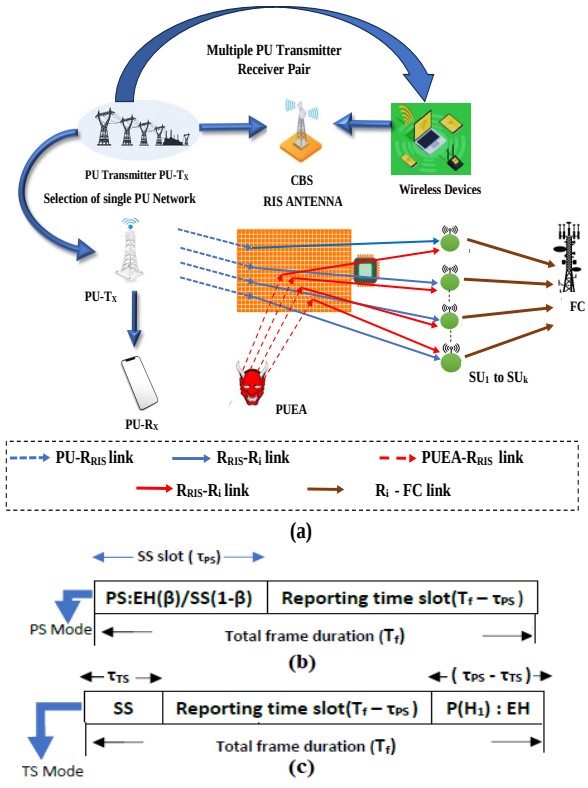

Fig. 1: (a) System model of RIS enabled EH-CSS, Frame structure, for (b) PS and (c) TS mode

Fig. 1 (a) shows the system model for EH-CSS based CR network using RIS antenna where multiple PU transmitter-receiver pairs, K collocated AF SUs/cognitive relays (R_is) [6], one unfriendly jammer in the form of PUEA and a fusion center (FC) are present. PU network consists of 'K_p' number of transmit-receive pairs and is governed by a central base station (CBS) as shown in Fig. 1 (a). Although, multiple PU transmitter-receiver pair are considered, only one pair seems to be operative equi-probably at a time slot governed by CBS for simplicity of mathematical analysis.

Fig. 1 (b) and Fig. 1(c) show the frame structure of PS and TS mode, respectively. In PS mode (in Fig. 1(b)), the communication time line is divided into two different non-overlapping time slots, a SS/sampling slot (τ_{PS}) and a reporting slot ($T_f - \tau_{\text{PS}}$). Within τ_{PS}, each SU_i senses 'N' number of samples of both PU and PUEA signal received via RIS. RIS antenna basically acts like a relay between the PU and/or PUEA and SU. RIS reflects the signals with some desired angles that can be tuned by FC. In PS mode of operation, the received signal from RIS to the SUs are divided into power ratio of $\beta_i : (1-\beta_i)$, where β_i and $(1-\beta_i)$ are used to facilitate EH and SS processes, respectively [6].

TS scheme, as shown in Fig. 1(c), operates in three sequential slots, one for SS (τ_{TS}), reporting slot ($T_f - \tau_{\text{PS}}$), and an EH slot ($\tau_{\text{PS}} - \tau_{\text{TS}}$) [6]. In both PS and TS modes, during the reporting slot ($T_f - \tau_{\text{PS}}$), SUs (SU_i $i \in [1,k]$) amplify and forward the received signal from RIS with a gain factor (ϱ) to the FC. This facilitates the synthesis of a global CSS decision like in [6]. Notably, EH at 'SUs' within the TS configuration exclusively occurs during PU transmission intervals, once the global CSS decision is finalized [6].

A. Signal Analysis and Channel Modeling using RIS

The received signal at SU_i during τ_{PS} can be written as

$$Y_{su_i}(n) = \varphi h_{pr_i} h_{r_i,su_i} X_{pr}(n) + h_{mr_i} h_{mr_i,su_i} X_{mr}(n) + v_{su_i}(n) \quad (1)$$

Here, n= 1 to N. The symbols 'N' and 'f_s' denote the number of samples and sampling frequency, respectively. The channel fading coefficients, mentioned as h_{r_i,su_i} and h_{mr_i,su_i} in Eq. (1), show the impact of RIS antenna at the receiver of SU_i.

Probabilities of PU's transmit and non-transmit states are given by $\mathcal{P}(\mathcal{H}_1) = \mathcal{P}(\varphi = 1)$ and $\mathcal{P}(\mathcal{H}_0) = \mathcal{P}(\varphi = 0)$, respectively [10]. In PS mode, the signal received at each SU_i is divided as $Y_{suh_i}(n) = \beta Y_{su_i}(n)$ and $Y_{sus_i}(n) = (1-\beta)Y_{su_i}(n)$, respectively, for EH and SS purposes, where $\beta_i = \beta$ [10]. For TS mode (Fig. 1 (c)), entire portion of $Y_{su_i}(n^{'})$ is used for SS, where $n^{'}$ = 1 to $N^{'}$ and $N^{'} = \tau_{\text{TS}} f_s$.

Symbols $X_{pr}(n)$ and $X_{mr}(n)$ denote the signal of PU and PUEA, respectively and their analysis is similar as reported in [6], [10]. PU and PUEA power for transmitting their signals are denoted by P_p and P_m, respectively. Additive noise signal and its variance at each SU_i are denoted by the symbols $v_{su_i}(n)$ and σ_n^2, respectively. Modeling of noise is done similarly as done in [10]. In Eq. (1), PUEA signal is transmitted over PU band and is impaired by the channel gain (second term) unlike the total noise term at the receiver of SU_i (third term), [6]. Furthermore, P_p and P_m values are

comparable and relatively larger than the noise variance. Thus PUEA signal acts an interfering RF signal at SU_i to the desired PU signal [6] and can be utilized for the purpose of harvesting as done using the PU signal. FC finally combines the total signal received during (T_f-τ_{PS}) for both PS and TS mode and mentioned respectively as given below

$$Y_C^{PS}(n) = \sum_{i=1}^{K} \sqrt{\varrho_i} h_{su_i,c}\ Y_{su_i}(n) + v_c(n) \tag{2}$$

$$Y_c^{TS}(n^{'}) = \sum_{i=1}^{K} \sqrt{\varrho_i} h_{su_i,c} Y_{su_i}(n^{'})) + v_c(n^{'}), \tag{3}$$

Here n = 1 to $\tau_{\text{PS}} f_s$ and $n^{'}$ = 1 to $\tau_{\text{TS}} f_s$. The noise at the FC is denoted by v_c with zero mean and variance σ_c^2 [6].

B. Distant dependent fading model between PU/PUEA and SU via RIS antenna

Let h_{pr_i}, h_{mr_i}, h_{r_i,su_i}, h_{mr_i,su_i} and $h_{su_i,c}$ be the fading channel coefficients considering the links from PU to the i^{th} RIS element ($PU - R_i$), PUEA to the i^{th} RIS element ($PUEA - R_i$), the i^{th} RIS element to the i^{th} SU ($r_i - su_i$) for reflecting the PU signals, the i^{th} RIS element to the i^{th} SU ($mr_i - su_i$) for reflecting the PUEA signals, and the i^{th} SU to fusion center ($su_i - c$), respectively. The fading coefficient is modeled as $h_m \sim \mathcal{CN}(0, d_m^{-\alpha_m})$, where the distance between any two nodes and the coefficient of path loss are denoted by the symbols 'd' and 'α', respectively with $m \in \{pr_i, mr_i, (r_i, su_i), (mr_i, su_i)(su_i, c)\}$. Furthermore, h_{r_i,su_i} and h_{mr_i,su_i} are given by $\mathcal{A}e^{-j\Theta_{r_i,su_i}}$ and $\mathcal{B}e^{-j\Theta_{mr_i,su_i}}$, respectively where $\mathcal{A}$, $\mathcal{B}$, Θ_{r_i,su_i} and Θ_{mr_i,su_i} represent the amplitude of RIS reflected path from PU, amplitude for PUEA, phase part for PU and phase part from PUEA, respectively.

Due to mathematical tractability, the present work models the channel fading coefficients as $|h_{r_i,su_i}|^2 = |\mathcal{A}e^{-j\Theta_{r_i,su_i}}|^2 \sim \mathcal{CN}(0, d_{r_i,su_i}^{-\alpha_{r_i,su_i}})$ and $|h_{mr_i,su_i}|^2 = |\mathcal{B}e^{-j\Theta_{mr_i,su_i}}|^2 \sim \mathcal{CN}(0, d_{mr_i,su_i}^{-\alpha_{mr_i,su_i}})$. Here the fading gain is developed as zero mean and variance in the form $d_m^{-\alpha_m}$ which is dependent on distance between PU/PUEA to RIS and RIS to SU. Hence the placement of RIS in between PU/PUEA transmitter and SU plays a pivotal role in the calculation of overall RE.

C. CSS and Energy Consumption using RIS

The symbols T_{st}^{PS} and T_{st}^{TS} represent the test statistics at FC for PS and TS mode, respectively and are evaluated similarly as in [6]. Here $d_{pr_i} = d_{pr}$, $d_{mr_i} = d_{mr}$, $d_{r_i,su_i} = d_{rsu}$, $d_{mr_i,su_i} = d_{mrsu}$, $d_{su_i,c} = d_{suc}$, $\varrho_i = \varrho$ ($\forall\ i = 1, ..K$) as in [10].

Mean values of T_{st}^{PS} for hypotheses $\mathcal{H}_0$ and $\mathcal{H}_1$, respectively are given as $E(T_0) = \tau_{\text{PS}} f_s \mu_0$ and $E(T_1) = \tau_{\text{PS}} f_s \mu_1$ respectively, and the same for T_{st}^{TS} considering hypotheses $\mathcal{H}_0$ and $\mathcal{H}_1$ are $E(T_0^{'}) = \tau_{\text{TS}} f_s \mu_0^{'}$ and $E(T_1^{'}) = \tau_{\text{TS}} f_s \mu_1^{'}$, respectively [6]. Here $\mu_1 = (1-\beta)K\varrho r_1 + \sigma_c^2$, $\mu_0 = (1-\beta)K\varrho r_0 + \sigma_c^2$, $\mu_1^{'} = K\varrho r_1 + \sigma_c^2$, $\mu_0 = K\varrho r_0 + \sigma_c^2$, $r_0 = d_{mr}^{-\alpha_{mr}} d_{mrsu}^{-\alpha_{mrsu}} d_{suc}^{-\alpha_{suc}} P_m + d_{suc}^{-\alpha_{suc}} \sigma_c^2$ and $r_1 = d_{pr}^{-\alpha_{pr}} d_{rsu}^{-\alpha_{rsu}} d_{suc}^{-\alpha_{suc}} P_p + r_0$. The variance of T_{st}^{PS} under $\mathcal{H}_1$ and $\mathcal{H}_0$ are $Var(T_1) \approx \tau_{\text{PS}} f_s \mu_1^2$, $Var(T_0) \approx \tau_{\text{PS}} f_s \mu_0^2$, respectively and the same for T_{st}^{TS} under hypotheses $\mathcal{H}_0$ and $\mathcal{H}_1$ are $Var(T_0^{'}) \approx \tau_{\text{PS}} f_s (\mu_0^{'})^2$ and $Var(T_1^{'}) \approx \tau_{\text{TS}} f_s (\mu_1^{'})^2$, respectively [6].

The detection and false alarm probabilities considring the test statistics for both PS and TS based EH are calculated similarly as reported in [6]. In order to function SS and/or EH, some small power is required in the internal circuit of SUs and is given by P_{s_i}. The total energy consumption for PS during τ_{TS} is given by $E_{ST}^{PS} = KP_s\tau_{\text{PS}}$. The same for TS mode, during τ_{TS} and (τ_{PS}-τ_{TS}), are given by $E_{ST_1}^{TS} = KP_s\tau_{\text{TS}}$ and $E_{ST_2}^{TS} = KP_s(\tau_{\text{PS}}$-$\tau_{\text{TS}})\mathcal{D}$, respectively, where $P_{s_i} = P_s$ ($\forall i$=1 to K) and $\mathcal{D} = P_d\mathcal{P}(\mathcal{H}_1) + P_f\mathcal{P}(\mathcal{H}_0)$. All K SUs forward their received signal samples to the FC during τ_{PS} and τ_{TS}, using energies $E_C^{PS} = (1-\beta)K\varrho S\tau_{\text{PS}}$ and $E_C^{TS} = K\varrho S\tau_{\text{TS}}$, respectively, where $S = \Big\{\mathcal{P}(\mathcal{H}_1) d_{pr}^{-\alpha_{pr}} d_{rsu}^{-\alpha_{rsu}} P_p + d_{mr}^{-\alpha_{mr}} d_{mrsu}^{-\alpha_{mrsu}} P_m + \sigma_n^2\Big\}$.

III. RE calculation and Problem Formulation

Here also we adopted NL-EH model as mentioned in [6]. K number of SUs harvest energy during τ_{PS} and τ_{TS} and are given by $E_H^{PS} = K\Phi_{\text{EH}}^{\text{PS}}\tau_{\text{PS}}$ and $E_H^{TS} = K\Phi_{\text{EH}}^{\text{TS}}(\tau_{\text{PS}}$-$\tau_{\text{TS}})$, respectively [6], where $\Phi_{\text{EH}}^{\text{PS}}$ and $\Phi_{\text{EH}}^{\text{TS}}$ are determined by putting P_ξ (in Eq. (5) [6]) as βS and $S^{'} = \Big\{P_d\mathcal{P}(\mathcal{H}_1)\Big(d_{pr}^{-\alpha_{pr}} d_{rsu}^{-\alpha_{rsu}} P_p + d_{mr}^{-\alpha_{mr}} d_{mrsu}^{-\alpha_{mrsu}} P_m + \sigma_n^2\Big) + P_f\mathcal{P}(\mathcal{H}_0)\ \Big(d_{mr}^{-\alpha_{mr}} d_{mrsu}^{-\alpha_{mrsu}} P_m + \sigma_n^2\Big)\Big\}$, respectively. Here EH is done from the received RF signal power of PU and PUEA.

Total RE calculated considering PS and TS modes are shown in Eqs. (9) and (10), respectively, where $\mathcal{A}_1 = (\Phi_{EH}^{TS} - P_s\mathcal{D})\tau_{\text{PS}}$ and $\mathcal{B}_1 = (\Phi_{EH}^{TS} + P_s(1-\mathcal{D}))$.

A. Problem Formulation with Optimal Solutions

The symbol $\mathbf{C_1}$ denotes the constraint for detection of the PU and is given by $P_d \geq \overline{P}_d$, $P_f \leq \overline{P}_f$, where $\overline{P}_d$ and $\overline{P}_f$ are the predefined detection and false alarm probabilities, respectively. Each SU maintains an energy causality constraint. This ensures non-negative RE at individual SU_i. The energy causality constraint, considering PS and TS based EH operations, are given by $\mathbf{C_2^{PS}}$:$(\Phi_{\text{EH}}^{\text{PS}} - ((1-\beta)\varrho S + P_s))\tau_{\text{PS}} \geq 0$ and $\mathbf{C_2^{TS}}$:$(\mathcal{A}_1 - (\mathcal{B}_1 + \varrho S)\tau_{\text{TS}}) \geq 0$, respectively ($\because d_{pr_i} = d_{pr}$, $d_{mr_i} = d_{mr}$, $d_{r_i,su_i} = d_{rsu}$, $d_{mr_i,su_i} = d_{mrsu}$, $d_{su_i,c} = d_{suc}$, $\varrho_i = \varrho$, $P_{s_i} = P_s\ \forall\ i = 1, 2, ...K$) [10].

Inclusion of RIS aided EH operation for PS and TS modes, lead to the optimization problems as mentioned below

$$\max_{K,\varrho,\tau_{\text{PS}},\beta} \Big(\Phi_{\text{EH}}^{\text{PS}} - ((1-\beta)\varrho S + P_s)\Big) K\tau_{\text{PS}} \text{ s.t. } \mathbf{C_1}, \mathbf{C_2^{PS}} \tag{4}$$

$$\max_{K,\varrho,\tau_{\text{TS}}} K(\mathcal{A}_1 - (\mathcal{B}_1 + \varrho S)\tau_{\text{TS}}) \qquad \text{s.t. } \mathbf{C_1}, \mathbf{C_2^{TS}} \tag{5}$$

Following the argument in [6], $P_d = \overline{P}_d$ and $P_f = \overline{P}_f$ are made for both in PS and TS mode, as given below

$$\mathbf{C_1^{PS}} :(1-\beta)K\varrho\Big(\Omega + (r_0 - r_1)\sqrt{\tau_{\text{PS}} f_s}\Big) + \sigma_c^2\mathcal{B} = 0 \tag{6}$$

$$\mathbf{C_1^{TS}} :K\varrho\Big(\Omega + (r_0 - r_1)\sqrt{\tau_{\text{TS}} f_s}\Big) + \sigma_c^2\mathcal{B} = 0 \tag{7}$$

where $\Omega = r_0\mathcal{Q}^{-1}(\overline{P}_f) - r_1\mathcal{Q}^{-1}(\overline{P}_d)$, $\mathcal{B} = \mathcal{Q}^{-1}(\overline{P}_f) - \mathcal{Q}^{-1}(\overline{P}_d)$.

B. Objective Function using RIS and its Solution

The objective functions using RIS-EH, considering both PS and TS mode, are expressed as $\mathcal{O}_{\mathcal{F}}^{PS}$ and $\mathcal{O}_{\mathcal{F}}^{TS}$ (in Eqs. (4) and (5)), respectively. Since $\Phi_{\text{EH}}^{\text{PS}}$ in Eq. (4) is a function of β, for mathematical tractability and obtaining its optimal value, $\mathcal{O}_{\mathcal{F}}^{PS}$ needs to be modified. Following the same argument reported in [6] as $P_\xi = \beta S$ and $\exp(-a(P_\xi - b))$=$\exp(-a(\beta S - b)) \approx 1 - a(\beta S - b)$ ($\because |a(\beta S - b)| < 1$ and ignoring the rest higher order terms) in Eq. (4), we can write

$$\Phi_{\text{EH}}^{\text{PS}}(\beta) = \frac{\frac{\lambda}{2-a(\beta S-b)} - \frac{\lambda}{1+\exp(ab)}}{1 - \frac{1}{1+\exp(ab)}} \implies \frac{\frac{\lambda}{(2+ab)-a\beta S} - \mathcal{F}_1}{\mathcal{F}_2}$$
$$\implies \frac{\lambda}{\mathcal{F}_2}\frac{1}{(q_1 - \beta q_2)} - \Big(\frac{\mathcal{F}_1}{\mathcal{F}_2}\Big) \implies \frac{\mathcal{F}_3}{(q_1 - \beta q_2)} - \mathcal{F}_4 \quad (13)$$

where, the symbols P_ξ and λ denote the total RF power received and the constant maximum harvested power at each SU when saturation condition occurs for EH, respectively [6]. Furthermore, $\mathcal{F}_3 = \frac{\lambda}{\mathcal{F}_2}$, $\mathcal{F}_4 = \frac{\mathcal{F}_1}{\mathcal{F}_2}$, $q_1 = (2+ab)$ and $q_2 = aS$.

Using Eq. (13), energy causality constraint as mentioned in Eq. (4) and the objective function can be re-written as $\mathbf{C_{2m}^{PS}}$: $(\frac{\mathcal{F}_3}{(q_1-\beta q_2)} - ((1-\beta)\varrho S + \mathcal{C}))\tau_{\text{PS}} \geq 0$ and $\mathcal{O}_{\mathcal{F}}^{PS}$=$(\frac{\mathcal{F}_3}{(q_1-\beta q_2)} - ((1-\beta)\varrho S + \mathcal{C}))K\tau_{\text{PS}}$, respectively where, $\mathcal{C}$=$(\mathcal{F}_4 + P_s)$. Henceforth considering the PS mode, the optimization problem as given in Eq. (4) can be rewritten as

$$\max_{K,\varrho,\tau_{\text{PS}},\beta} \Big(\frac{\mathcal{F}_3}{(q_1 - \beta q_2)} - ((1-\beta)\varrho S + \mathcal{C})\Big)K\tau_{\text{PS}}$$
$$\text{s.t. } i)\ \mathbf{C_1^{PS}},\ \ ii)\ \mathbf{C_{2m}^{PS}} \quad (14)$$

Using Lagrange method, the analytical solutions of optimization problems in Eqs. (5) and (14) are made. $\mathcal{L}^{\text{PS}}$ and $\mathcal{L}^{\text{TS}}$, respectively are the Lagrangian functions for both PS and TS modes as mentioned in Eq. (10). The symbols μ_1 and μ_2 are the Lagrange multiplier. Optimal solutions to Eq. (10) using both PS and TS modes of EH are evaluated using Karush-Kuhn-Tucker (KKT) conditions as mentioned in Eqs. (11) and (12), respectively [6], where, $a_1 = (r_0 - r_1)\sqrt{f_s}$, $b_1 = \frac{\mathcal{F}_3}{(q_1-\beta_{\text{PS}}^* q_2)} - \mathcal{C}$, $c_1 = 3\Omega(1-\beta_{\text{PS}}^*)a_1 - \sigma_c^2\mathcal{B}$, $d_1 = 4(1-\beta_{\text{PS}}^*)\sigma_c^2\mathcal{B}S^2$, $e_1 = 3\Omega(1-2\beta_{\text{PS}}^*)(r_1 - r_0) + \sigma_c^2\mathcal{B}$, $f_1 = b_1 - (1-\beta_{\text{PS}}^*)\varrho_{\text{PS}}^* S$, $g_1 = 2(\Omega)^2\sigma_c^2\mathcal{B}(\Omega\mathcal{B}_1 - \mathcal{A}_1 a_1^2) - \mathcal{A}_1 a_1^2 f_s S$, $h_1 = 3\Omega a_1$, $X_{11} = 4h_1\mathcal{C}q_2$, $Y_{11} = h_1(2\mathcal{F}_3 + 3\mathcal{C}q_2)$, $Z_{11} = h_1(2\mathcal{F}_3 + \mathcal{C}q_1) + \sigma_c^2\mathcal{B}(\mathcal{C}(q_1 - q_2) - 2\mathcal{F}_3)$. Here the symbols $\mathcal{D}$ and $S^{'}$, mentioned in $\mathcal{A}_1$ and $\mathcal{B}_1$, are calculated using $P_d = \overline{P}_d$, $P_f = \overline{P}_f$. K_{PS}^* and K_{TS}^* are rounded off to the nearest integer in order to obtain a tractable solution.

1) Analysis on RE without PUEA: In PUEA absence, SU_i forwards the reflected signal from PU to RIS as given below

$$Y_{su_i}^{'}(n) = \varphi h_{pr_i} h_{r_i,su_i} X_{pr}(n) + v_{su_i}(n) \quad (15)$$

In absence of PUEA, all mathematical expressions, for finding the solutions to the optimization problems in Eqs. (5) and (14) are similar; however, the expressions of r_0, S and $S^{'}$ are modified as r_0= $d_{suc}^{-\alpha_{suc}}\sigma_c^2$, S=$\Big\{\mathcal{P}(\mathcal{H}_1)d_{pr}^{-\alpha_{pr}}d_{rsu}^{-\alpha_{rsu}}P_p + \sigma_n^2\Big\}$, $S^{'}$=$\Big\{P_d\mathcal{P}(\mathcal{H}_1)\Big(d_{pr}^{-\alpha_{pr}}d_{rsu}^{-\alpha_{rsu}}P_p + \sigma_n^2\Big) + P_f\mathcal{P}(\mathcal{H}_0)\sigma_n^2\Big\}$.

IV. Numerical Results

Simulation results are obtained by taking average over 10000 independent iterations. The parameters involved in simulation are mentioned as [6]: $\overline{P}_d = 0.95$, $\overline{P}_f = 0.1$, $T_f = 10$ ms, $f_s = 150\ KHz$, $\mathcal{P}(\mathcal{H}_0) = 0.7$, $\mathcal{P}(\mathcal{H}_1) = 0.3$ $P_p = 4\ mW$, $P_s = 1\ mW$, $P_m = 2.5\ mW$, $\sigma_n^2 = \sigma_c^2 = 0.05\ mW$, $d_{pr} = 1.58$ m, $d_{mr} = 1.2$ m, $d_{rsu} = 1.6m$, $d_{mrsu} = 1.4m$, $d_{suc} = 1.4$ m, $\alpha_{pr} = \alpha_{rsu} = \alpha_{mrsu} = \alpha_{mr} = \alpha_{suc} = 4$, $a = 1500$, $b = 0.0022$, $\lambda = 24\ mW$, [6], [10].

In Fig. 2 (a), the impact of the total number of SUs (K) on RIS based E_{res}^{PS} and E_{res}^{TS} along with the comparative study over [6] is reported in presence of PUEA. The nature of the graph and the explanation for concavity is similar as mentioned in [6]. Here also, as reported in [6], we can see that E_{res}^{TS} [with PUEA] $> E_{res}^{PS}$ [with PUEA] i.e. performance of TS based RIS-EH is found superior to that of PS mode w.r.t RE. However, the values of E_{res}^{TS} and E_{res}^{PS} in presence of PUEA using RIS antenna are significantly larger compared to that of [6]. E_{res}^{TS} [with PUEA] attains a maximum value of 2.862 mJ (almost more than 10 times compared to [6]) at $\{K_{\text{PS}}^* = 17, \beta_{\text{PS}}^* = 0.6523, \varrho_{\text{PS}}^* = 1.3915, \tau_{\text{PS}}^* = 0.3719\ ms\}$, whereas E_{res}^{PS} [with PUEA] is 2.786 mJ at $\{K_{\text{TS}}^* = 18, \varrho_{\text{TS}}^* = 3.4553, \tau_{\text{TS}}^* = 0.1684\ ms\}$. Simulation and analytical results match well and values found of $\varrho_{\text{PS}}^*, \varrho_{\text{TS}}^* > 1$. At $K = 12$, about 45% and 38.97% gain for both PS and TS mode, respectively are observed in the proposed RIS based E_{res} as compared to the same reported in [6].

A comparative analysis on total RE for both PS and TS

$$E_{res}^{PS} = E_H^{PS} - (E_C^{PS} + E_{ST}^{PS}) = \Big(K\Phi_{\text{EH}}^{\text{PS}}\tau_{\text{PS}} - ((1-\beta)K\varrho S\tau_{\text{PS}} + KP_s\tau_{\text{PS}})\Big) = \Big(\Phi_{\text{EH}}^{\text{PS}} - ((1-\beta)\varrho S + P_s)\Big)K\tau_{\text{PS}} \quad (8)$$

$$E_{res}^{TS} = E_H^{TS} - E_C^{TS} - E_{ST_1}^{TS} - E_{ST_2}^{TS} = \Big(K\Phi_{\text{EH}}^{\text{TS}}(\tau_{\text{PS}} - \tau_{\text{TS}}) - (K\varrho S\tau_{\text{TS}} + KP_s(\tau_{\text{TS}} + (\tau_{\text{PS}} - \tau_{\text{TS}})\mathcal{D})\Big) = K(\mathcal{A}_1 - (\mathcal{B}_1 + \varrho S)\tau_{\text{TS}}) \quad (9)$$

$$\mathcal{L}^{\text{PS}} = \Big(\frac{\mathcal{F}_3}{(q_1 - \beta q_2)} - ((1-\beta)\varrho S + \mathcal{C})\Big)K\tau_{\text{PS}} + \mu_1 C_1^{\text{PS}} + \mu_2 C_{2m}^{\text{PS}}, \quad \mathcal{L}^{\text{TS}} = K(\mathcal{A}_1 - (\mathcal{B}_1 + \varrho S)\tau_{\text{TS}}) + \mu_1 C_1^{\text{TS}} + \mu_2 C_2^{\text{TS}} \quad (10)$$

$$\beta_{\text{PS}}^* = \frac{Y_{11} + \sqrt{Y_{11}^2 - 4X_{11}Z_{11}}}{2X_{11}}, \varrho_{\text{PS}}^* = \frac{2b_1c_1 + d_1}{(1-\beta_{\text{PS}}^*)Se_1}, K_{\text{PS}}^* = \frac{2a_1\Big(\frac{f_1}{S} - (1-\beta_{\text{PS}}^*)(2S - \frac{\varrho_{\text{PS}}^*}{2})\Big)}{3\Omega^2(\varrho_{\text{PS}}^*)^3(1-\beta_{\text{PS}}^*)^2\sigma_c^2\mathcal{B}}, \tau_{\text{PS}}^* = \Big[\frac{(1-\beta_{\text{PS}}^*)K_{\text{PS}}^*\varrho_{\text{PS}}^*\Omega + \sigma_c^2\mathcal{B}}{(1-\beta_{\text{PS}}^*)K_{\text{PS}}^*\varrho_{\text{PS}}^* a_1}\Big]^2 \quad (11)$$

$$\varrho_{\text{TS}}^* = \frac{-g_1 + \sqrt{g_1^2 + 8(\Omega)^4\sigma_c^2\mathcal{B}S\mathcal{A}_1\mathcal{B}_1 a_1 f_s}}{2(\Omega)^4\sigma_c^2\mathcal{B}S}, K_{\text{TS}}^* = \frac{2\Omega^3\sigma_c^2\mathcal{B}(\varrho_{\text{TS}}^* S + \mathcal{B}_1)}{\varrho_{\text{TS}}^*\Big(\Omega(\varrho_{\text{TS}}^* S + \mathcal{B}_1) - \mathcal{A}_1 a_1\sqrt{f_s}\Big)}, \tau_{\text{TS}}^* = \Big[\frac{K_{\text{TS}}^*\varrho_{\text{TS}}^*\Omega + \sigma_c^2\mathcal{B}}{K_{\text{TS}}^*\varrho_{\text{TS}}^* a_1}\Big]^2 \quad (12)$$

TABLE I: Comparative analysis on total RE (E_{res}) using RIS for PS and TS modes over [6]

EH mode	PUEA power (mW)	Optimal Parameter Set				$\mathcal{P}(\mathcal{H}_1)$	Total Harvested Energy (mJ)	Total Energy Consm. (mJ)	Total RE Proposed (mJ)	Total RE in [6] (mJ)
		K^*	ϱ^*	β^*	τ^*_{PS} / τ^*_{TS} (ms)					
PS	no PUEA	8	1.152	0.6526	τ^*_{PS}=0.6521	0.25	2.3456	0.8963	1.4493	0.0925
TS	no PUEA	10	3.5852	-	τ^*_{TS}=0.1752	0.25	2.2568	0.9664	1.2904	0.0639
PS	P_m= 2.5 mW	9	2.7591	0.6213	τ^*_{PS}=0.6842	0.25	2.4458	1.1254	1.3204	0.0756
TS	P_m= 2.5 mW	9	4.8521	-	τ^*_{TS}=0.1954	0.25	2.3954	1.1452	1.2502	0.0435
PS	no PUEA	8	1.0598	0.6851	τ^*_{PS}=0.6194	0.35	3.0492	1.1651	1.8841	0.1341
TS	no PUEA	10	3.2983	-	τ^*_{TS}=0.1664	0.35	2.9338	1.2563	1.6775	0.9265
PS	P_m= 2.5 mW	9	2.5374	0.6652	τ^*_{PS}=0.6495	0.35	3.1795	1.4631	1.7164	0.1096
TS	P_m= 2.5 mW	9	4.4589	-	τ^*_{TS}=0.1797	0.35	3.1142	1.4887	1.6253	0.0631

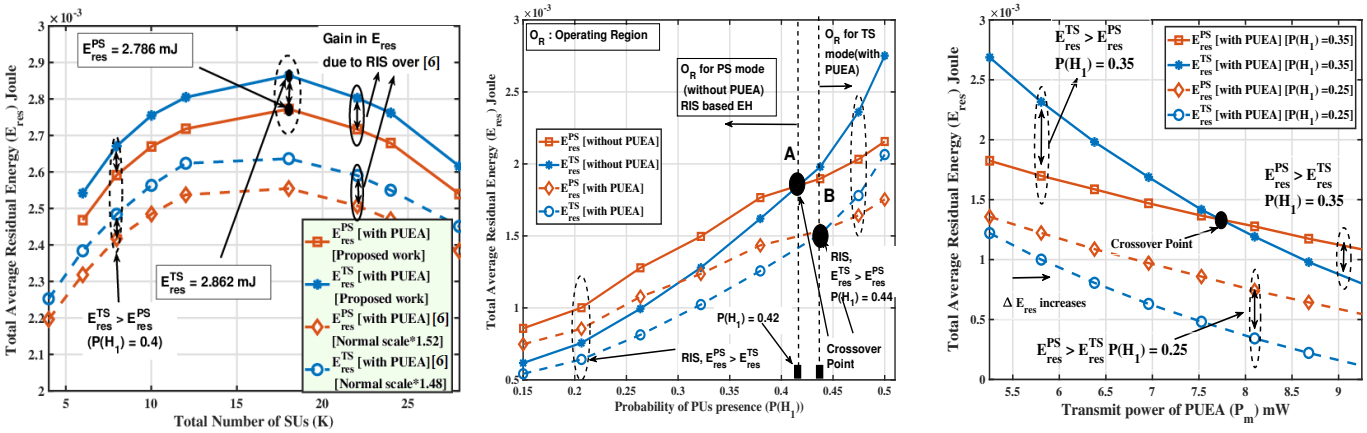

Fig. 2: Total average residual energy ($E_{residue}$) versus a) K; b) $\mathcal{P}(\mathcal{H}_1)$; c) P_m (mW)

mode of EH for the proposed RIS based approach and the same reported in [6] at $\mathcal{P}(\mathcal{H}_1) = 0.25$ and $\mathcal{P}(\mathcal{H}_1) = 0.4$, in absence and presence of PUEA, are mentioned in Table I. It is clearly observed that though energy consumption (to meet target SS reliabilities), is increased using RIS antenna compared to [6], the total harvested energy is significantly more which in turn gives an overall benefit in total RE over [6]. For RIS based PS mode of EH, in absence of PUEA at $\mathcal{P}(\mathcal{H}_1) = 0.25$ and $\mathcal{P}(\mathcal{H}_1) = 0.35$, total RE are $\sim$15.67 and $\sim$14.05 times more compared to [6]. On the contrary, considering TS mode in presence of PUEA ($P_m = 2.5mW$), at $\mathcal{P}(\mathcal{H}_1) = 0.25$ and $\mathcal{P}(\mathcal{H}_1) = 0.35$, total RE are $\sim$28.74 and $\sim$25.76 times more compared to [6].

Fig. 2 (b) illustrates the operating region of both PS and TS modes by clearly depicting the crossing points considering the cases of absence and presence of PUEA as in [6]. 'A' and 'B' are the crossing points observed at $\mathcal{P}(\mathcal{H}_1) = 0.42$ and $\mathcal{P}(\mathcal{H}_1) = 0.44$, respectively considering the cases of absence and presence of the PUEA. The main aim of these results is to claim the benefit of using RIS over [6]. A gain $\sim$11.31% in E^{PS}_{res} over E^{TS}_{res} at $\mathcal{P}(\mathcal{H}_1) = 0.3$ in absence of PUEA, whereas $\sim$10.85% in E^{TS}_{res} over E^{PS}_{res} in presence of PUEA at $\mathcal{P}(\mathcal{H}_1) = 0.4$ are found using RIS. Hence it can be concluded that the favorable operating region using RIS antenna for PS mode without and with PUEA are found to be $\mathcal{P}(\mathcal{H}_1)$ = 0.15 to 0.42 and 0.15 to 0.44, respectively. On the contrary favorable operating region for TS mode without and with PUEA are found to be $\mathcal{P}(\mathcal{H}_1)$ =0.42 to 0.5 and 0.44 to 0.5, respectively.

Fig. 2 (c) shows the impact of PUEA transmit power (P_m) on E_{res} for PS and TS mode. Here also a crossing point is observed at $P_m = 7.65\ mW$ and after that it is seen that $E^{PS}_{res} > E^{TS}_{res}$. When the value of P_m is increased, both τ_{PS} and τ_{TS} values also increase. With the increment in the value of τ_{PS}, RIS facilitates in EH process (as shown in Fig. 1 (b)), however, for the same increment in τ_{TS}, the possibility of harvesting reduces (as shown in Fig. 1 (c)). For $\mathcal{P}(\mathcal{H}_1)$ = 0.25, $E^{PS}_{res} > E^{TS}_{res}$, a gradual increment in the gap is observed with the increase in P_m value.

A. Impact on RE value with change in the placement of RIS antenna near/far to PU in absence of PUEA

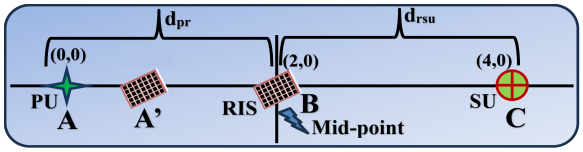

Fig. 3: Impact on E_{res} with change in placement of RIS antenna near/far w.r.t. PU in absence of PUEA

The impact on E_{res} value for PS and TS mode in absence of PUEA with the change in RIS antenna near/far to PU is discussed here. It is assumed initially that the RIS antenna is placed in the middle of PU and SU transmitter ('B' point) as shown in Fig. 3. The total distance between PU and SU i.e. D_p is fixed to 4 meters such that $D_p = d_{pr} + d_{rsu} = 4mt$. It is assumed that PU, RIS and SU_i are placed at coordinates (0,0), (2,0) and (4,0), respectively. Since all SUs are assumed

to be collocated and $d_{pr_i} = d_{pr}$, $d_{r_i,su_i} = d_{rsu}$, $d_{su_i,c} = d_{suc}$ [6], [10], the location of all the SUs are considered to be fixed at point 'C' i.e approx (4,0). Let us now assume that the RIS antenna is placed to a new position A'. Here $d_{pr} < 2$ implies RIS antenna is placed near to PU and far from SU transmitter. Simulation for Fig. 4 is done for $P_p = 5mW$ and $P_p = 10mW$ and by setting $\mathcal{P}(\mathcal{H}_0) = 0.75$, $\mathcal{P}(\mathcal{H}_1) = 0.25$, $\alpha_{pr} = 3.5, \alpha_{rsu} = \alpha_{suc} = 4$ while other remaining parameters are kept same as mentioned earlier.

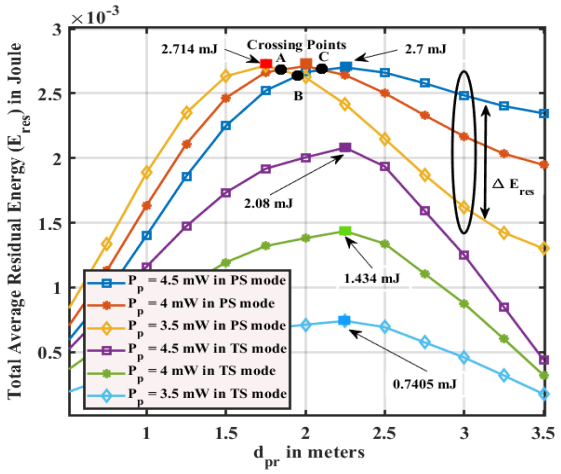

Fig. 4: E_{res} without PUEA using RIS versus d_{pr}

It is observed in Fig. 4 that with the increase in d_{pr} value from 0.5 meters to 3.5 meters, E_{res} value increases for both PS and TS mode. Another interesting fact in the observation from Fig. 4 is that the maximum value of E_{res}^{PS} is not exactly at the middle i.e. $d_{pr} = 2$ meters, rather the same for $P_p = 3.5mW$, $P_p = 4mW$ and $P_p = 4.5mW$ are found to be 2.714 mJ, 2.71 mJ and 2.7 mJ at $d_{pr} = 1.75$ meters, $d_{pr} = 2.03$ meters and $d_{pr} = 2.25$ meters, respectively. Crossing points **A**, **B** and **C** are observed at $x_p = 1.82$ meters, $d_{pr} = 1.95$ meters and $d_{pr} = 2.1$ meters, respectively. This implies that E_{res}^{PS} value is more (EH is more) for low transmit power i.e. $P_p = 3.5mW$ compared to higher transmit power i.e. $P_p = 4.5mW$ when RIS antenna is placed near to PU transmitter. Furthermore it also implies that if RIS antenna is placed away from PU i.e. $d_{pr} > 2.5$ meters, E_{res}^{PS} value is more for $P_p = 4.5mW$ compared to the case for $P_p = 4mW$ and $P_p = 3.5mW$. When d_{pr} value is increased beyond 1.5 meters, the values of β and ρ both reduce. This is turn reduces the harvested energy (less value in β) and increases the energy consumption for lower P_p i.e. 3.5 mW relative to higher value of the same i.e for 4.5 mW (about 34.83% less at $d_{pr} = 3$ meters). It is observed that the maximum values of E_{res}^{TS} are found to be 0.7405 mJ, 1.434 mJ and 2.08 mJ at $d_{pr} = 2.25$ meters and are 72.71%, 47.08%, 22.96% less compared to E_{res}^{PS} for $P_p = 3.5mW$, $P_p = 4mW$ and $P_p = 4.5mW$, respectively for $\mathcal{P}(\mathcal{H}_1) = 0.25$.

V. Conclusion and Future Works

This paper aims to enhance the network lifetime of the cognitive users by proposing a switch mode RIS-EH operation in CSS in presence of multiple PUs. The optimal solutions for amplifying gain, total number of SUs, time duration for sensing of PS and TS mode and PS ratio (for PS mode) are derived to maximize the total RE while maintaining a target detection and false alarm probability alongwith individual energy causality constraints. At $K = 12$, the present work using RIS-EH achieved a gain in E_{res} of about 45% and 38.97% for PS and TS mode compared to [6]. It is observed that the value of E_{res}^{PS} is more for $P_p = 3.5mW$ compared to $P_p = 4.5mW$ when RIS antenna is placed near to PU transmitter. The maximum value of E_{res}^{PS} in absence of PUEA for $P_p = 3.5mW$, $P_p = 4mW$ and $P_p = 4.5mW$ are found to be 2.714 mJ, 2.71 mJ and 2.7 mJ at $d_{pr} = 1.75$ meters, $d_{pr} = 2.03$ meters and $d_{pr} = 2.25$ meters, respectively. It is also observed that the maximum values of E_{res}^{TS} are found to be 0.7405 mJ, 1.434 mJ and 2.08 mJ at $d_{pr} = 2.25$ meters and are 72.71%, 47.08%, 22.96% less compared to E_{res}^{PS} for $P_p = 3.5mW$, $P_p = 4mW$ and $P_p = 4.5mW$, respectively for $\mathcal{P}(\mathcal{H}_1) = 0.25$.

References

[1] Y. Gu and S. Aïssa, "RF-based energy harvesting in decode-and-forward relaying systems: Ergodic and outage capacities," *IEEE Trans. on Wireless Commun.*, vol. 14, no. 11, pp. 6425–6434, Nov. 2015.

[2] S. Aslam, W. Ejaz, and M. Ibnkahla, "Energy and spectral efficient cognitive radio sensor networks for internet of things," *IEEE Internet of Things Journal*, vol. 5, no. 4, pp. 3220–3233, Aug 2018.

[3] N. Agrawal, A. Bansal, K. Singh, C.-P. Li, and S. Mumtaz, "Finite block length analysis of RIS-assisted UAV-based multiuser iot communication system with non-linear EH," *IEEE Trans. on Commun.*, vol. 70, no. 5, pp. 3542–3557, 2022.

[4] M. Nitti, M. Murroni, M. Fadda, and L. Atzori, "Exploiting social internet of things features in cognitive radio," *IEEE Access*, vol. 4, pp. 9204–9212, 2016.

[5] S. Chatterjee, A. Banerjee, T. Acharya, and S. P. Maity, "Fuzzy c-means clustering in energy detection for cooperative spectrum sensing in cognitive radio system," in *Multiple Access Communications*, (Cham), pp. 84–95, Springer Intern. Publishing, 2014.

[6] A. Banerjee and S. P. Maity, "On residual energy maximization in cooperative spectrum sensing with PUEA," *IEEE Wireless Commun. Lett.*, vol. 8, no. 6, pp. 1563–1566, 2019.

[7] A. Alahmadi, Z. Fang, T. Song, and T. Li, "Subband PUEA detection and mitigation in OFDM-based cognitive radio networks," *IEEE Trans. on Infor. Forensics and Security*, vol. 10, no. 10, pp. 2131–2142, 2015.

[8] K. Hsieh, F. Tseng, and M. Ku, "A spectrum and energy cooperation strategy in hierarchical cognitive radio cellular networks," *IEEE Wireless Commun. Lett.*, vol. 5, no. 3, pp. 252–255, June 2016.

[9] A. Banerjee, A. Paul, and S. P. Maity, "Joint power allocation and route selection for outage minimization in multihop cognitive radio networks with energy harvesting," *IEEE Trans. on Cognitive Commun. and Netw.*, vol. 4, no. 1, pp. 82–92, March 2018.

[10] A. Banerjee and S. P. Maity, "Jamming in eavesdropping on throughput maximization in green cognitive radio networks," *IEEE Trans. on Mobile Comp.*, vol. 22, no. 1, pp. 299–310, 2023.

[11] Y. Huang and Y. Zou, "Upper-bound ergodic capacity analysis of RIS-aided energy-harvesting relay systems," in *IEEE Global Commun. Conf.*, pp. 3235–3240, 2022.

[12] N. Sharma and S. Gautam, "Optimizing RIS-assisted wireless communication systems with non-linear energy harvesting," in *Proc. 5th Intern. Conf. on Energy, Power and Environment: Towards Flexible Green Energy Technologies (ICEPE)*, pp. 1–5, 2023.

[13] H. Alakoca, M. Babaei, L. Durak-Ata, and E. Basar, "RIS-empowered non-linear energy harvesting communications over nakagami-m channels," *IEEE Commun. Lett.*, vol. 26, no. 9, pp. 2215–2219, 2022.

[14] P. K. Sharma, N. Sharma, S. Dhok, and A. Singh, "RIS-assisted FD short packet communication with non-linear EH," *IEEE Commun. Lett.*, vol. 27, no. 2, pp. 522–526, 2023.